Geophysical Research Letters

RESEARCH LETTER
10.1029/2019GL084896

Effective Rheology Across the Fragmentation Transition for Sea Ice and Ice Shelves

J.A. Åström[1] and D.I. Benn[2]

[1]CSC - IT Centre for Science, Esbo, Finland, [2]School of Geography and Sustainable Development, University of St Andrews, St Andrews, Scotland

Key Points:
- A high-resolution first-principles ice fracture model is employed to determine an effective rheology for ice that undergoes fragmentation
- A sharp transition occurs between an elastic-brittle solid and a viscous fluid, in contrast to many damage models of ice
- The fragmentation transition may be a key factor determining the stability of thinning ice shelves

Supporting Information:
- Supporting Information S1

Correspondence to:
J. A. Åström,
astrom@csc.fi

Citation:
Åström, J. A., & Benn, D. I. (2019). Effective rheology across the fragmentation transition for sea ice and ice shelves. *Geophysical Research Letters*, *46*. https://doi.org/10.1029/2019GL084896

Received 8 AUG 2019
Accepted 18 SEP 2019

Abstract Sea ice and ice shelves can be described by a viscoelastic rheology that is approximately linear elastic and brittle at high strain rates and viscously shear thinning at low strain rates. Brittle ice easily fractures under compressive shear and forms shear bands as the material undergoes a transition to a fragmented, granular state. This transition plays a central role in the mechanical behavior at large scales of sea ice in the Arctic Ocean or Antarctic ice shelves. Here we demonstrate that the fragmentation transition is characterized by an essentially discontinuous drop of three to five orders of magnitude in effective viscosity and stress relaxation time. Beyond the fragmentation transition, grinding in shear zones further reduces both effective viscosity and shear stiffness, but with an essentially constant relaxation time of ~10 s. These results are relevant for ice rheology implementation in large-scale climate-related models of sea ice and thin ice shelves.

Plain Language Summary Models of ice dynamics adopt various parameterizations of the material properties of ice. These parameterizations define a rheology for ice that may include viscous, plastic, elastic, and/or brittle behavior. Using a combination of theory and a discrete element model which by construction does not require a prescribed rheology, we find that an abrupt transition occurs as fracture density increases, with sudden drops in shear strength and effective viscosity separating low and high fracture states. The existence of this transition has important implications for, for example, understanding the stability of ice shelves and their ability to "buttress" the flow of inland ice, and for the development of continuum models for the dynamics of sea ice at the geophysical scale.

1. Introduction

In ice sheet and glacier models, ice is typically treated as a continuous medium with viscous rheology and constant density. In several important glaciological contexts, however, the behavior of ice is dominated by discontinuous processes, such as brittle fracture and granular flow. Calving from tidewater glaciers, avalanching from hanging glaciers, and ice flow during surges are all dependent upon discontinuous processes (Benn et al., 2017; Pralong & Funk, 2005; Riikilä et al., 2015). Additionally, the ability of floating ice shelves to buttress inland ice is strongly influenced by accumulated fracture in lateral shear margins (e.g., Borstad et al., 2016; Sun et al., 2017), and weakening and fragmentation of ice shelves are recognized as a key process affecting the stability of the West Antarctic Ice Sheet (Pollard et al., 2015; Scambos et al., 2017). Methods for calculating the strength and rheology of fragmented ice can therefore significantly enhance our ability to predict the response of glaciers and ice sheets to oceanic and atmospheric warming.

Modeling efforts for sea ice have differed significantly from those for glacier ice. For the obvious reason that sea ice tends to be highly fragmented, the early elastic-plastic rheological model (Coon et al., 1974) was intended to account for fragmented ice by modeling it as a plastic material beyond a critical stress state. In order to extend modeling to sea ice drift and jamming at a critical thickness, Hibler introduced the viscous-plastic rheology (Hibler, 1979). To include brittle fracture, Girard et al. introduced the elastic-brittle rheology (Girard et al., 2009), which can account for the heterogeneous nature of brittle sea ice but lacks viscous stress relaxation. Recently, this was added to the elastic-brittle rheology in the Maxwell elastic-brittle model that includes elastic, brittle, and viscous components that can capture both intermittency and heterogeneity of sea ice fracture (Dansereau et al., 2016).

The rheology of fractured ice can, at least in principle, be determined from observations of surface ice velocity data using inversion techniques (e.g., Borstad et al., 2012, 2016; Vieli et al., 2007). Because

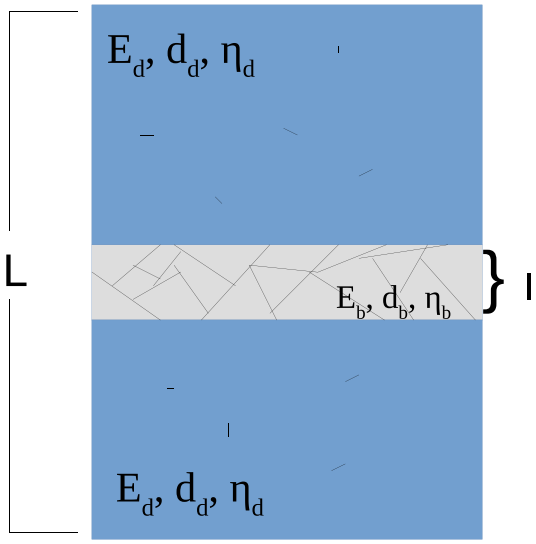

Figure 1. A schematic representation of the theoretical model: a fragmented zone of width l and larger areas of size L with, more or less, intact ice with some diffuse fracture. The different parameters for stiffness (E), viscosity (η), and damage (d) with subscript d, in the areas with diffuse fracture, and, in the fragmented zone with, subscript b are indicated.

the degree of fracture evolves through time, snapshots derived from inversions become increasingly unreliable in simulations where ice configuration or dynamics deviate significantly from the initial state. For prognostic simulations, therefore, a first-principles approach without a prescribed rheology would be useful. Here, we employ theoretical arguments and the Helsinki Discrete Element Model (HiDEM) to find an effective viscoelastic rheology of thin ice shelves and sea ice across the transition from an intact viscoelastic solid to fragmented, granular material.

2. An Effective Rheology for Ice Across the Fragmentation Transition

Our objective is to construct an effective rheology for sea ice and thin ice shelves as they under compressive stresses undergo a transition from intact or mildly fractured to a highly fragmented granular state, like drift ice. This type of rheology is in sharp contrast to the rheology needed to model, for example, a single rift slowly propagating across an ice shelf. In such a case, the transient stress relaxation via creep, flow, and elastic deformations around the crack tip needs to be modeled in detail, as well as the criterion for crack advancement (see, e.g., Lipovsky, 2018; Rist et al., 1999; Sinha, 1988; Sunder & Wu, 1990). In contrast we view ice as a material that can exist in states ranging from intact or mildly damaged to highly fragmented with orders of magnitude variations in effective stiffness and viscosity.

To create such a rheology for geophysical scale ice models, it is important to mimic real fracture events on realistic spatial and temporal scales. Effective rheology is size and time scale dependent, and we therefore concentrate on a length scale relevant for discretization in continuum ice models (i.e., 1−10 km) and on a time scale relevant for fracture. With these considerations in mind, we can formulate an effective viscoelastic rheology for thin shelves and sea ice across the fragmentation transition. For simplicity and following previous progressive damage approaches (Kachanov, 1958), we describe in our model the degree of fragmentation of the ice at the microscopic scale through a mesoscopic scalar damage variable, d, the value of which we set to 1 for an undamaged and 0 for ice so fragmented that it can flow freely without much further fracturing. We consider a 2-D ice body of size L. This ice body has large regions with little or diffuse damage (i.e., almost intact ice) and regions of intense damage (i.e., cracks and shear bands). These are assumed to have width l and typically extend over the entire domain L once the fragmentation transition is surpassed. A sketch of the configuration can be found in Figure 1. If this ice body is strained across the shear band or crack, we can write effective strain, ε, as $\varepsilon L = \varepsilon_d\,(L - l) + \varepsilon_b l$, where ε_b is strain in the shear band/crack and ε_d is strain in the diffuse damage regions. We further define d_b as the damage parameter in shear bands. Similarly, d_d is the diffuse damage parameter. If we then write a simple Hooke's law stress balance across the shear band as $S_b\varepsilon_b = S_d\varepsilon_d$, where S is a stiffness modulus (i.e., S can be the Young's (E), shear (G), or bulk (K) modulus), we get for an effective stiffness modulus of the ice:

$$S = S_b \Big/ \left[\frac{l}{L} + \left(\frac{S_b}{S_d}\right)\left(1 - \frac{l}{L}\right)\right]. \tag{1}$$

Similarly, for effective viscosity, η, we get

$$\eta = \eta_b \Big/ \left[\frac{l}{L} + \left(\frac{\eta_b}{\eta_d}\right)\left(1 - \frac{l}{L}\right)\right]. \tag{2}$$

We regain stiffness and viscosity S_d and η_d for $l = 0$ or $d_b = d_d$ (which imply that $S_d = S_b$ and $\eta_d = \eta_b$) and S_b and η_b for $l = L$, as we should. The damage parameter for the entire ice block can be written as

$$d = d_d \frac{(L-l)}{L} + d_b \frac{l}{L}. \quad (3)$$

To construct the rheology, we further need to know how S and η depend on d_d and d_b. A straightforward mean-field approach, which should be valid for small damage (d_d, $d_b \sim 1$) would give $S_d = S_0 d_d$, $S_b = S_0 d_b$ and $\eta_d = S_0 d_d$, $\eta_b = \eta_0 d_b$, where S_0 and η_0 are constants (cf. Dansereau et al., 2016; Riikilä et al., 2015). A typical fragmentation process proceeds as follows. Initially there is no shear band and $l = 0$. Then, S_d and η_d both decrease linearly with decreasing d_d, until eventually an instability is reached at $d_d = d_{frac}$ and a shear band is formed. At this point, d_d stagnates, and d_b vanishes rapidly. For a small l/L, there will not be much change in d when this happens, and therefore almost discontinuous drops in both $S(d)$, and $\eta(d)$ will be the result. It is interesting to notice that the appearance of the near discontinuous drop does not even require a precise definition of stiffness and viscosity as function of the damage parameter.

In other words, this scenario defines a rheology that is not very sensitive to the exact form of $S(d)$ and $\eta(d)$ but more sensitive to the localization of damage and deformation in a shear band or crack. The occurrence of localization, however, sets limits on what $S(d)$ and $\eta(d)$ can be. Fracture appears in solids but not in fluids, so for $d \approx 1$ we must have a long viscous relaxation time defined by η/S. That is, $\eta/S \gg 1$ s. When fractures appear, stress should be relaxed rapidly and irreversibly to allow for crack propagation and thus localization. This means that, for some d, η/S should be much smaller. Dansereau et al. (2016) realized this in the context of sea ice, by prescribing $E = E_0 d$ and $\eta = \eta_0 d^\alpha$, with $1 < \alpha < 7$, with $\alpha = 4$ as perhaps an optimal value. Some additional distinctions must be made whether $S = E$, G, or K. For unidirectional tensile fracture, a single spanning crack is enough to erase all possibility of elastic stress transfer. In equations (1)–(3), this is described by $l/L \to 0$ and $S_b = 0$, and $\eta_b = 0$, at the instant, a spanning tensile crack appears. This means, without any change in d at the transition point, stiffness and viscosity drop discontinuously to zero. In contrast, compressive shear fracture leads to the formation of shear bands, which have a nonzero l. A fragmented shear band under compression will have a significant residual stiffness, E, G, or K, but a strongly reduced viscosity compared to undamaged ice. We thus expect a significant drop in the relaxation time, but not such a large reduction in E in this case. Once a shear band has formed, stress relaxes rapidly by irreversible flow, and grinding of ice fragments continues, which further lowers both viscosity and stiffness. We can describe this residual stiffness behavior using the simplest possible ansatz: $\partial S/\partial d \propto -S$, leading to a postfragmentation exponential decay of S (Riikilä et al., 2015). Postfragmentation, η, should behave in a roughly similar fashion as a function of d.

At the fragmentation transition, we would expect a critical regime in which the viscosity is described by a power law divergence $\eta \propto (d_{frac} - d)^{-\gamma}$, where γ is a critical exponent. The connectivity, that is, the average number of unbroken beams/particle in the HiDEM simulations (Åström et al., 2013) in the shear bands, decreases rapidly at the fragmentation transition and crosses the rigidity threshold, which is the same as the percolation threshold for the current model (Thorpe & Duxbury, 2003). As rigidity is lost in shear bands, it is lost for the entire structure. The exponent γ is not known, however. It should be vaguely related to, for example, the exponent in the Krieger and Dougherty (1959) equation, which relates a divergent viscosity of a liquid-solid suspension to the solid volume fraction or the fraction of aggregated particles (Starov et al., 2002). In our case, the process is the reverse of aggregation—it is the fragmentation of solid clusters into smaller pieces.

3. HiDEM Simulations

In order to test the validity of the above rheology, we employed a discrete element numerical model for ice fracture (HiDEM; Åström et al., 2013). The model is constructed of spherical elements connected by breakable Euler-Bernoulli beams with a square cross section of width 0.6 times the particle diameters. The damage parameter in the DEM model thus becomes the fraction of unbroken beams. The elastic stress, and thereby the fracture criterion, in HiDEM is a function of the tension/compression of a beam and the rotations of the linked DEMs relative to the axis of the beam. As most yield or fracture criteria, the HiDEM criterion is a sum of a tensile/volumetric term and a deviatoric term. The first term is proportional to the stretching of the beam and the second includes shear, bending, and torsion of the beam defined by the rotations. For simplicity, the latter deformation modes are not separated but merged into a single term defined by the absolute

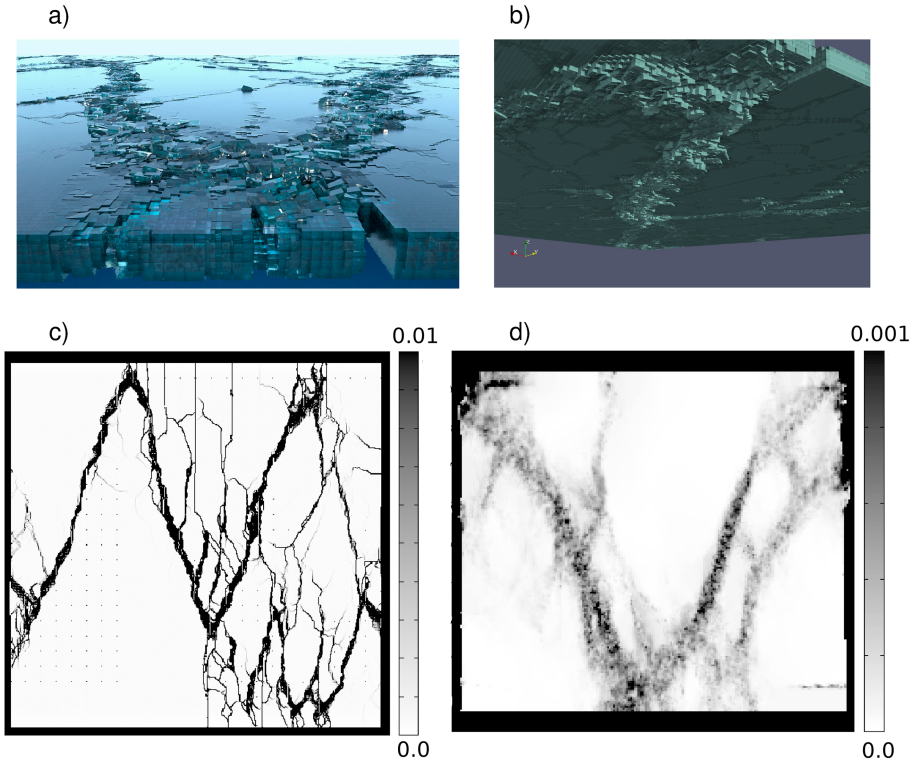

Figure 2. (a) A perspective snapshot of the results of a HiDEM sea ice fragmentation simulation. The model discretization of ice blocks is visible. (b) The same ice below sea surface. (c) A grayscale strain map. Large strain/fractures displayed in black (strain ~0.01) and intact ice in white. (d) Corresponding strain map for a ~100-m-thick ice shelf. Strain scales and size in km indicated on the axis.

value of the difference between rotation angles of the end points of a beam times a variable proportionality constant. A value of 0.35 gave rise to shear bands and compression ridges often observed for sea ice (cf. Figures. 2a and 2b). A smaller value caused the ice to buckle without breaking. The fracture criterion can furthermore be defined either as an instantaneous fracture, which means that the particle-particle interaction mediated by a beam vanish in a single time step if the fracture criterion is fulfilled. HiDEM also allows for more gradual fractures, for example, strain softening or plasticity. We only used the instantaneous criteria.

We used DEM particle of sizes in the range 1–10 m and defined the model domain in terms of two horizontal (x, y) and one vertical (z) axes. Boundary conditions were chosen such that in the y direction, compressive stress on the boundary was gradually increased with time, $\sigma_y = (S/L)\,(\Delta y - t\dot{\varepsilon}L)$, where S is again a stiffness constant, Δy is boundary displacement, $\dot{\varepsilon}$ is strain rate, and t is time. In the x direction a constant pressure was applied on all ice outside the original geometry. In the vertical (z) direction, ice floats at minimal potential energy on the water surface constrained by buoyancy and gravity. With these boundary conditions, deformations remained close to reversible. That is, if $t \rightarrow -t$, the ice would return roughly to its original shape, although the formation of pressure ridges would be an exception. Effective shear stiffness, G, was measured as $G = (\sigma_y - \sigma_x)/(\varepsilon_y - \varepsilon_x)$ and effective viscosity as $\eta = (\sigma_y - \sigma_x)/(\dot{\varepsilon}_y - \dot{\varepsilon}_x)$. These cannot be measured simultaneously: fast loading (i.e., compared to η/E) can be used to measure G and slow loading to measure η. Measuring both separately is not a problem for intact ice, but to measure it across the fragmentation transition is problematic because neither effective viscosity nor stiffness is well defined for a fragmented material. That is, effectively measured η and E would depend on, for instance, the mode and direction of loading, as well the length and time scales that are employed. The most reasonable approach in such a case is to mimic the type, size, and speed of deformations usually observed in nature for the particular case of interest and simply use the definitions above to obtain a useful rheology.

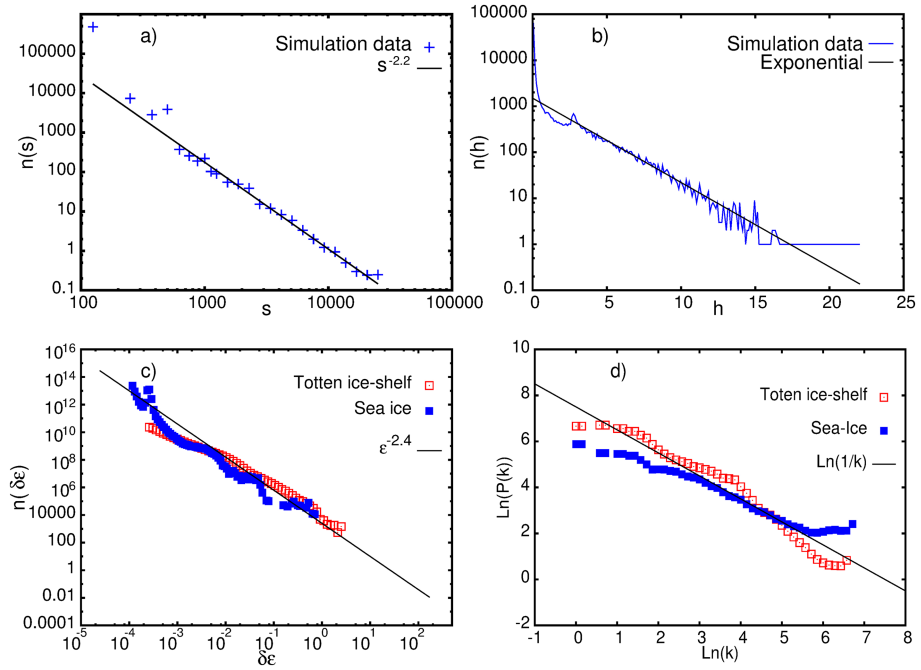

Figure 3. (a) A fragment size distribution $n(s)$ for sea ice compared to a power law. (b) Keel-depth distribution, $n(h)$. (c) Strain rate distribution s, $n(\delta\varepsilon)$. (d) Spatial power spectrum, $P(k)$, for frequencies k measured in 1/m.

We compute effective η and G for square domains of size $L^2 \sim 10$–100 km^2, which were broken by compressive shear after roughly 1 hr of linearly increasing load to reach roughly ~10% effective strain. This particular setup was chosen because it represents typical domain dimensions in large-scale sea ice (Dansereau et al., 2016) and ice shelf models (Sun et al., 2017). We tested two cases: ice that was 1- to 10-m thick, which is a good model for Arctic sea ice, and ice 100- to 200-m thick, representative of thin Antarctic ice shelves. Figure 2 shows the results of a HiDEM sea ice fragmentation simulation, viewed from the surface (Figure 2a) and beneath (Figure 2b). Figure 2c shows the strain map for the same ~20 km^2 square of sea ice, with narrow and straight vertical tension cracks and broad, uneven, and diagonal shear bands. Figure 2d shows a similar map for an ice shelf. The much larger thickness of the shelf makes depth averaged shear bands look more diffuse. Fragments are formed in two categories: small fragments that are created by grinding in shear zones and large pieces of more or less unbroken ice between the shear zones and tensile cracks.

For benchmarking HiDEM results in the sea ice case, fragment size distributions $n(s)$, strain rate distributions $n(\dot{\varepsilon})$, fracture field power spectra $P(k)$, and ridge height distribution $n(h)$ are compared with observations. Fragment size distributions, $n(s)$, should be dominated by fragments that form within shear bands by grinding. We would then expect $n(s) \propto s^{-\gamma}$, with $\gamma \sim 1.7$ to 3.5, depending on the amount of grinding (Sulak et al., 2017). This is in agreement with observations (Matsushita, 1985; Rothrock & Thorndike, 1984; Weiss & Marsan, 2004). Strain rate distributions, $n(\dot{\varepsilon}) \propto \varepsilon^{-\beta}$, have been measured for sea ice at spatial and temporal resolutions of 10 km and 3 days, respectively, with $\beta \sim 2.4$ (Girard et al., 2009; Marsan et al., 2004). The third benchmark, spatial power spectra of the fragmented ice, was extracted from satellite images for which white ice and dark sea water were easily distinguishable. The power spectra were found to obey approximately $1/f$ noise Weiss & Marsan, 2004), a result that seems to be fairly universal for brittle fragmentation (Leary, 2002). Fragments within compressive shear zones in sea ice do not typically stay within the plane of the ice, but ridges form both above and below the sea surface (Figures 2a and b). The height, h, distributions of these ridges and keels have been observed to follow exponentials, $n(h) \propto \exp(-const * h)$ (Rothrock & Thorndike, 1980; Tan et al., 2012; Wadhams, 1988). HiDEM results for glacier and shelf calving can be found in Åström et al. (2014), Benn et al. (2017), and Cook et al. (2018).

In Figure 3, we display comparisons between the simulations and observations. Simulation results are for a similar setup as in Figure 2, and, as additional benchmarking, we also display HiDEM results for a few

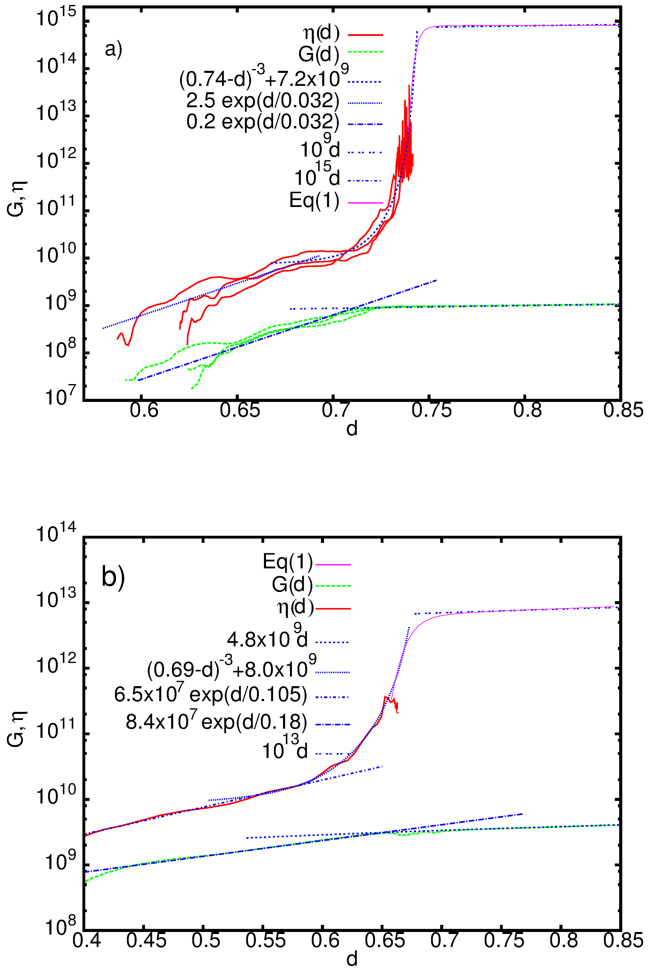

Figure 4. (a) The viscoelastic rheology described by $\eta(d)$ and $G(d)$ for ~10-m-thick sea ice. In the intact phase $G \sim 10^9 d$ [N/m^2] and $\eta \sim 10^{15} d$ [Ns/m^2]. The fragmentation transition appears at $d \approx 0.74$. The postfragmentation exponential behavior, power law decay of η at the transition, and equations (1) and (2) are compared to simulation results for three separate simulations. (b) Same as in (a) but for a ~100-m-thick ice shelf.

glaciers (Benn & Åström, 2018). Figure 3a displays the fragment size distributions, $n(s)$. The numerical results are fitted with a power law $n(s) \propto s^{-2.2}$. Figure 3b shows the keel-depth distribution $n(h) \propto exp(-h/2.25)$. Figure 3c shows the strain distribution, $n(\Delta\varepsilon)$, in the fragmented phase, where $\Delta\varepsilon$ is the local change strain over ~30 s during numerical simulations. The results are compared to the power law, $n(\Delta\varepsilon) \propto \Delta\varepsilon^{-2.4}$. Figure 3d shows the spatial power spectrum of fracture patterns such as those as displayed in Figure 2a. Results are displayed for sea ice and Totten ice shelf (Cook et al., 2018). It is evident from these plots that the HiDEM model can consistently reproduce observed behavior of sea ice and ice shelves.

In Figure 4 we compare $G(d)$ and $\eta(d)$ to the theoretical estimates (equations (1)–(3)) for both sea ice and shelf ice. Figure 4a displays the results of three separate sea ice runs. The prefragmentation effective stiffness and viscosity are quite well described by $G = G_0 d$ and $\eta = \eta_0 d$. As expected, there is no significant discontinuous drop in G at the fragmentation transition, and a crossover to exponential decay, $G \propto \exp(const \cdot d)$, is observed. In contrast, the fragmentation transition drop in η for sea ice is about five orders of magnitude and is well described by equation (2) with $l/L \approx 0.02$, matching the shear band width shown in Figure 2a. The drop in viscosity for the ice shelf case is about an order of magnitude smaller, which also matches the wider shear bands observed on shelves. It should also be noted that it takes a larger value of damage to trigger the fragmentation transition for the thicker ice shelf. At the transition, there seems to be, as expected, a critical regime in which the viscosity is described by a power law divergence $\eta \propto (d_{frac} - d)^{-3}$.

4. Conclusions

Fragmentation transitions in ice are extremely efficient in relaxing stress. This is true for both shear zones and tensile cracks. This phenomenon manifests itself in an inherent temporal asymmetry in the mechanical behavior of sea ice: Stress relaxation is very fast during fracture events, which may be followed by slow refreezing and stress buildup. This fracture behavior naturally leads to marginal stability and scale invariance, consistent with observations (Marsan et al., 2004; Weiss, 2013). Dansereau et al. (2016) discussed the same asymmetry. The effects of efficient stress relaxation can also be seen in large velocity gradients across fractured shear margins in glaciers and ice shelves. Fractured shear margins can support stress only in compression, with important implications for ice shelf buttressing.

From a modeling point of view, our results mean that viscoelastic ice rheology can be linked to a discretization scale L via the parameter l/L, where l is the characteristic width of fragmented shear zones. Here it should be pointed out that the typical width of a fragmented zone is far from a trivial parameter. For example, a tensile fracture is formed as thin crack but may expand to become very wide. This is evident, for example, in the scale invariant distribution of the widths of leads (Marcq & Weiss, 2012). In our model l corresponds to the width of the initial crack. That is defined by the "volume" of the fragmented ice that created the crack or shear band. It is still unclear, however, how a characteristic crack width l could be unambiguously obtained. A problematic case for our proposed rheology would be when drift ice becomes so fragmented that separation of individual compression ridges becomes impossible. The parameter l should be defined as the width of individual compression ridges and L as the separation between them. As l/L approach unity, it would become difficult to determine.

It is useful to compare our results to those of Dansereau et al. (2016) and Sun et al. (2017). Dansereau et al. developed a sea ice model based on the so-called Maxwell viscoelastic model, which includes both fracture

and healing. Their model links damage to viscosity and elasticity, which both increase and decrease with fracture and refreezing, respectively. The model is constructed so that elastic deformation dominates for intact or almost intact ice, while viscous deformations dominate in the opposite limit. If the ratio of stiffness and viscosity (i.e., the relaxation time) is chosen appropriately, the model can reproduce the main characteristics of sea ice mechanics, such as strain localization, anisotropy, intermittency, and associated scaling laws. This model is highly compatible with our model. Dansereau et al. used, as mentioned above, the functional relations: $\underline{E} = E_0 d$ and $\eta = \eta_0 d^{\alpha}$, with $1 < \alpha$, and $\eta_0/E_0 >> 1$ s. The motivation for these choices was to keep the model simple and to induce a decreasing relaxation time with increasing damage d. Our model results now suggest more detailed relations between stiffness, viscosity, and damage: When our damage parameter takes the value d_{frac}, it corresponds reasonably well to the parameter used by Dansereau et al. at $d = 0$. A proper parameter transformation allows for the implementation of additional dependence of G and η on d in the postfragmentation regime. Our results also suggest a relation between α and l/L, so that α would increase with increasing l/L. That is, the fragmentation transition approaches a discontinuity as $l \to 0$.

Sun et al. implemented a continuum damage model in the prognostic ice sheet model BISICLES to account for the effects of fracture. They parameterized damage from first principal stresses and then used a linear relation between damage and viscosity to account for the effects of fracture. This approach corresponds to our model with a constant stiffness in the regime above the fragmentation transition, with only limited and diffuse damage and viscosity proportional to damage. Although the model by Sun et al. is far simpler (and thereby easier to implement in large-scale flow models), it is likely to capture much of the relevant behavior of thicker ice shelves for which enhanced creep rather than fracture is likely to dominate deeper layers. This would cause a tendency for the ice shelf to remain largely in the diffuse damage regime where the model by Sun et al. generally coincides with ours.

Finally, we conclude that thinning of ice shelves, widely observed in Antarctica in recent decades, may have the effect of driving ice shelves toward the fragmentation transition. This could be a key factor in ice shelf collapse, which could act quite independently of climatically driven processes such as ponding of surface water and hydrofracturing. Furthermore, fragmentation transitions in thinning ice shelves could have devastating effects on ice shelf buttressing, even without a full collapse of the shelf. The results presented here could provide some insight into these issues.

Data files for the plots are found online (https://doi.org/10.5285/76D7D3CA-7B83-4BB0-AAE5-A8E92C7DA5B0) and in the Supporting Information S1.

References

Åström, J. A., Riikilä, T. I., Zwinger, T., Benn, D. I., Moore, J. C., & Timonen, J. (2013). A particle based simulation model for glacier dynamics. *The Cryosphere*, *7*, 1591–1602. https://doi.org/10.5194/tc-7-1591-2013

Åström, J. A., Vallot, D., Schäfer, M., Welty, E. Z., O'Neel, S., Bartholomaus, T. C., et al. (2014). Termini of calving glaciers as self-organized critical systems. *Nature Geoscience*, *7*(12), 874. https://doi.org/10.1038/ngeo2290

Benn, D. I., & Åström, J. A. (2018). Calving glaciers and ice shelves. *Advances in Physics X*, *3*, 1513819. https://doi.org/10.1080/23746149.2018.1513819

Benn, D. I., Åström, J. A., Zwinger, T., Todd, J., Nick, F. M., Cook, S., et al. (2017). *Journal of Glaciology*, *63*(240), 691–702. https://doi.org/10.1017/jog.2017.41

Borstad, C., Khazendar, A., Scheuchl, B., Morlighem, M., Larour, E., & Rignot, E. (2016). A constitutive framework for predicting weakening and reduced buttressing of ice shelves based on observations of the progressive deterioration of the remnant Larsen B Ice Shelf. *Geophysical Research Letters*, *43*, 2027–2035. https://doi.org/10.1002/2015GL067365

Borstad, C. P., Khazendar, A., Larour, E., Morlighem, M., Rignot, E., Schodlok, M. P., & Seroussi, H. (2012). A damage mechanics assessment of the Larsen B ice shelf prior to collapse: Toward a physically-based calving law. *Geophysical Research Letters*, *39*, L18502. https://doi.org/10.1029/2012GL053317

Cook, S., Åström, J. A., Zwinger, T., Galton-Fenzi, B. K., Greenbaum, J. S., & Coleman, R. (2018). Modelled fracture and calving on the Totten Ice Shelf. *The Cryosphere*, *12*, 2401–2411. https://doi.org/10.5194/tc-12-2401-2018

Coon, M. D., Maykut, G. A., Pritchard, R. S., Rothrock, D. A., & Thorndike, A. S. (1974). Modeling the pack ice as an elastic-plastic material. AIDJEX Bulletin, 24, Numerical Modeling Report, 1. University of Washington, Seattle.

Dansereau, V., Weiss, J., Saramito, P., & Lattes, P. (2016). A Maxwell elasto-brittle rheology for sea ice modelling. *The Cryosphere*, *10*, 1339–1359. https://doi.org/10.5194/tc-10-1339-2016

Girard, L., Weiss, J., Molines, J. M., Barnier, B., & Bouillon, S. (2009). Evaluation of high resolution sea ice models on the basis of statistical and scaling properties of Arctic sea ice drift and deformation. *Journal of Geophysical Research*, *114*, C08015. https://doi.org/10.1029/2008JC005182

Hibler, W. D. (1979). A dynamic thermodynamic sea ice model. *Journal of Physical Oceanography*, *9*, 815. https://doi.org/10.1175/1520-0485(1979)009<0815:ADTSIM>2.0.CO;2

Kachanov, L. (1958). Time of the rupture process under creep conditions. *Izvestiia Akademii Nauk SSSR, Otdelenie Teckhnicheskikh Nauk*, *8*, 26.

Krieger, I. M., & Dougherty, T. J. (1959). A mechanism for non-Newtonian flow in suspensions of rigid spheres. *Transactions. Society of Rheology*, *3*, 137.
Leary, P. C. (2002). Fractures and physical heterogeneity in crustal rock. In Heterogeneity of the crust and upper mantle—Nature, scaling and seismic properties. In J. A. Goff & K. Holliger (Eds.), (pp. 155–186). New York: Kluwer Academic/Plenum Publishers.
Lipovsky, B. P. (2018). Ice shelf rift propagation and the mechanics of wave-induced fracture. *Journal of Geophysical Research: Oceans*, *123*(6), 4014–4033. https://doi.org/10.1029/2017JC013664
Marcq, S., & Weiss, J. (2012). Influence of sea ice lead-width distribution on turbulent heat transfer between the ocean and the atmosphere. *The Cryosphere*, *6*(1), 143–156. https://doi.org/10.5194/tc-6-143-2012
Marsan, D., Stern, H., Lindsay, R., & Weiss, J. (2004). Scale dependence and localization of the deformation of Arctic sea ice. *Physical Review Letters*, *93*, 178501. https://doi.org/10.1103/PhysRevLett.93.178501
Matsushita, M. (1985). Fractal viewpoint of fracture and accretion. *Journal of the Physical Society of Japan*, *54*(3), 857–860. https://doi.org/10.1143/JPSJ.54.857
Pollard, D., DeConto, R. M., & Alley, R. B. (2015). Potential Antarctic ice sheet retreat driven by hydrofracturing and ice cliff failure. *Earth and Planetary Science Letters*, *412*, 112.
Pralong, A., & Funk, M. (2005). Dynamic damage model of crevasse opening and application to glacier calving. *Journal of Geophysical Research*, *110*, B01309. https://doi.org/10.1029/2004JB003104
Riikilä, T. I., Tallinen, T., Åström, J. A., & Timonen, J. (2015). A discrete-element model for viscoelastic deformation and fracture of glacial ice. *Computer Physics Communications*, *195*, 14.
Rist, M. A., Sammonds, P. R., Murrell, S. A. F., Meredith, P. G., Doake, C. S. M., Oerter, H., & Matsuki, K. (1999). Experimental and theoretical fracture mechanics applied to Antarctic ice fracture and surface crevassing. *Journal of Geophysical Research*, *104*(B2), 2973–2987.
Rothrock, D. A., & Thorndike, A. S. (1980). Geometric properties of the underside of sea ice. *Journal of Geophysical Research*, *85*, 3955.
Rothrock, D. A., & Thorndike, A. S. (1984). Measuring the sea ice floe size distribution. *Journal of Geophysical Research*, *89*(C4), 6477–6486. https://doi.org/10.1029/JC089iC04p06477
Scambos, T. A., Bell, R. E., Alley, R. B., Anandakrishnan, S., Bromwich, D. H., Brunt, K., et al. (2017). How much, how fast?: A science review and outlook for research on the instability of Antarctica's Thwaites Glacier in the 21st century. *Global and Planetary Change*, *153*, 16–34. https://doi.org/10.1016/j.gloplacha.2017.04.008
Sinha, N. K. (1988). Crack-enhanced creep in polycrystalline material: Strain-rate sensitive strength and deformation of ice. *Journal of Materials Science*, *23*(12), 4415–4428. https://doi.org/10.1007/BF00551940
Starov, V., Zhdanov, V., Meireles, M., & Molle, C. (2002). Viscosity of concentrated suspensions: Influence of cluster formation. *Advances in Colloid and Interface Science*, *96*, 279–293.
Sulak, D. J., Sutherland, D. A., Enderlin, E. M., Stearns, L. A., & Hamilton, G. S. (2017). Iceberg properties and distributions in three Greenlandic fjords using satellite imagery. *Annals of Glaciology*, *58*. https://doi.org/10.1017/aog.2017.5
Sun, S., Cornford, S. L., Moore, J. C., Gladstone, R., & Zhao, L. (2017). Ice shelf fracture parameterization in an ice sheet model. *The Cryosphere*, *11*(6), 2543–2554. https://doi.org/10.5194/tc-11-2543-2017
Sunder, S. S., & Wu, M. S. (1990). On the constitutive modeling of transient creep in polycrystalline ice. *Cold Regions Science and Technology*, *18*(3), 267–294. https://doi.org/10.1016/0165-232X(90)90025-R
Tan, B., Li, Z.-J., Lu, P., Haas, C., & Nicolaus, M. (2012). Morphology of sea ice pressure ridges in the northwestern Weddell Sea in winter. *Journal of Geophysical Research*, *117*, C06024. https://doi.org/10.1029/2011JC007800
Thorpe, M. F., & Duxbury, P. M. (Eds.) (2003). *Rigidity theory and applications*. Berlin: Springe-Verlag.
Vieli, A., Payne, A. J., Shepherd, A., & Du, Z. (2007). Causes of pre-collapse changes of the Larsen B ice shelf: Numerical modelling and assimilation of satellite observations. *Earth and Planetary Science Letters*, *259*(3-4), 297–306. https://doi.org/10.1016/j.epsl.2007.04.050
Wadhams, P. (1988). The underside of Arctic sea ice imaged by sidescan sonar. *Nature*, *333*(6169), 161–164. https://doi.org/10.1038/333161a0
Weiss, J. (2013). *Drift, deformation and fracture of sea ice—A perspective across scales*. Dordrecht: Springer.
Weiss, J., & Marsan, D. (2004). Scale properties of sea ice deformation and fracturing. *Comptes Rendus Physique*, *5*, 735. https://doi.org/10.1016/j.crhy.2004.09.005